IEEE Access
Multidisciplinary | Rapid Review | Open Access Journal

Received November 5, 2018, accepted November 23, 2018, date of publication November 27, 2018,
date of current version December 27, 2018.

Digital Object Identifier 10.1109/ACCESS.2018.2883530

Low-Complexity Spatial Parameter Estimation for Coherently Distributed Linear Chirp Source

LIANG ZHANG[1], YANBEI LIU[2], JIEXIAO YU[3], (Member, IEEE), AND KAIHUA LIU[3], (Member, IEEE)

[1]School of Computer Science and Technology, Civil Aviation University of China, Tianjin 300300, China
[2]School of Electronic and Information Engineering, Tianjin Polytechnic University, Tianjin 300387, China
[3]School of Electronic Information Engineering, Tianjin University, Tianjin 300072, China

Corresponding author: Liang Zhang (vfleon@163.com)

This work was supported in part by the Scientific Research Foundation of the Civil Aviation University of China under Grant 2017QD14X and in part by the National Science Foundation of China under Grant 61501322.

ABSTRACT In this paper, the problem of estimating the spatial parameters of multiple coherently distributed linear chirp sources is considered. In the fractional Fourier domain, a novel low-complexity algorithm based on the MUSIC criterion is proposed to estimate the central angle and the extension width. For small extension width scenarios, the 2-D spatial angle search in traditional estimators for the distributed sources estimation is replaced by a two-step 1-D MUSIC search which dramatically decreases the computational complexity. In the case of chirp signals with different frequency parameters, sources can be separated, and the spatial parameters of each source can be estimated individually. When sources cannot be separated, this problem can be considered as a classical direction-of-arrival estimation of multiple signals. In addition, the central angle estimation does not require any assumption on the distribution of angular spread. Simulation results show that the proposed algorithm obtains comparable performance in the parameters estimation accuracy for small extension width scenarios with the reduced complexity compared with our previous work.

INDEX TERMS Chirp signals, localization, fractional Fourier transform, MUSIC estimator.

I. INTRODUCTION

The direction of arrival (DOA) estimation problem of chirp sources for the far field point source model has been widely studied [1]–[3]. However, in many practical situations, the local scattering and reflection may result in angular spreading of the source energy. For example, significant angular scattering distributions can be observed in urban wireless communications [4]–[6]. In these scenarios, the transmitter is modeled as a spatially distributed source with a central angle and an extension width that is better than a point source, since angular spread may lead to inaccurate estimators using the point source model [6].

The application of classical distributed sources algorithms, such as the distributed source parameter estimator (DSPE) [6], the dispersed signal parametric estimation (DISPARE) [7] and the maximum likelihood (ML) estimator [8], leads to a multidimensional optimization of high computational cost. To reduce the complexity of estimation, a distributed source is approximated by a two-ray model in [9]. Then, the spatial parameters of the point sources are estimated by ROOT-MUSIC. Nonetheless, special approximations of the array covariance matrix may lead to bias estimates. The extended invariance principle (EXIP) algorithm [10] computes the central angle and the extension width in an efficient way by using two successive 1D searches. This algorithm is based on the single source assumption and cannot be extended to the multiple source case. In [11], a decoupled DOA estimator is proposed based on Generalized ESPRIT [12], which needs more sensors than MUSIC-type estimators. And MUSIC estimators generally outperform ESPRIT on the estimation performance. On the other hand, these algorithms consider single-frequency stationary signals as their incident sources, and require the steering vector be time-invariant. Thus, they cannot be used to estimate chirp signals, since time variable is introduced into steering vectors while receiving chirp signals.

In [13], we focused on coherently distributed (CD) chirp sources. Based on the fractional Fourier transform (FrFT), the steering vector in the dechirped domain was derived, in which the influence of the time parameter on the steering vector was eliminated when the received signals are non-stationary. Hence, spatial parameter estimation algorithms

TABLE 1. The definition of symbols.

Symbol	Definition
$(\square)^T$	the transpose
$(\square)^*$	the conjugate
$(\square)^H$	the conjugate transpose
$(\square)^{-1}$	the inverse
$E\{\square\}$	the statistical expectation operator
$\delta_{t_1 t_2}$	the Kronecker delta function
$\mathbf{I}$	the identity matrix
$\mathrm{tr}(\square)$	the matrix trace
$\lvert\square\rvert$	the matrix determinant
$\mathrm{Re}\{\square\}$	the real part of the matrix
$\square$	the Hadamard product operator

for distributed source, such as the conventional DSPE algorithm [6], can be extended to their counterparts in the dechirped domain. However, this estimator needs 2D spectral search.

To further reduce the complexity of our existing work, we propose a low-complexity spatial parameter estimation method on the basis of MUSIC estimator and give the Cramér-Rao bound (CRB) in this paper. Instead of using 2D search, a two-step 1D procedure is proposed.

Compared to classical distributed source schemes, the proposed algorithm has the following advantages:

1) The central angle estimation does not require any knowledge of the distribution of scattering rays, which is robust to mismodeling errors.

2) The proposed algorithm can even work in the case of the number of sources exceeds the number of sensors, while the sources are separable.

3) The deterministic angular signal density of incident sources can be different which is assumed to be identical for all sources in many traditional distributed source estimators.

4) The computational complexity of the proposed algorithm is much lower than that of traditional distributed source estimators while providing comparable performance.

The paper is organized as follows. In Section II, the definition of FrFT and some properties of chirp signals in the time-frequency domain are presented. In Section III, the models both in the time domain and in the fractional Fourier domain are reviewed. The proposed method is drawn and the CRB of the single source is addressed in Section IV. Simulation and analysis are given in Section V, and our conclusions are given in Section VI. Finally, the statistical property of signals in the fractional Fourier domain and the steering vector factorizing are derived in Appendix.

Some notations used throughout this paper are listed in Table 1, as follows:

II. FRACTIONAL FOURIER TRANSFORM

To provide the mathematical background, we rigorously define the FrFT in this section. Some properties of chirp signals in the time-frequency domain are explored as well.

A. DEFINITION OF FrFT

The FrFT is a generalized form of the conventional Fourier transform (FT), which reveals the variation tendency of each frequency component of signals over time in the time-frequency plane. The fractional Fourier domain contains both the time and frequency characteristics of transformed signals.

The mathematical definition of FrFT can be given through the following linear integral transform [14]–[16]

$$X(p,u) = F^p[x(t)] = \int_{-\infty}^{\infty} K_p(u,t)x(t)dt, \tag{1}$$

where $F^p[\cdot]$ denotes the FrFT operator of the pth order, kernel $K_p(u,t)$ is defined as

$$K_p(u,t) = \begin{cases} \sqrt{1-j\cot\alpha}\, e^{j\pi\left(t^2\cot\alpha - 2tu\csc\alpha + u^2\cot\alpha\right)}, & p \neq 2n \\ \delta(t-u), & p = 4n \\ \delta(t+u), & p = 4n \pm 2 \end{cases} \tag{2}$$

and n is an integer. Note that the fractional Fourier domain can be interpreted as it makes rotation angle $\alpha = p\pi/2$ with the time domain. For convenience, both the FrFT operators $F^p[\cdot]$ and $F^\alpha[\cdot]$ can be considered as equivalent in this paper.

B. PROPERTIES OF CHIRP SIGNALS IN THE FRACTIONAL FOURIER DOMAIN

The chirp signal we considered can be modeled as

$$x(t) = a_0 e^{j\pi(2f_0 t + \mu_0 t^2) + j\varphi_0}, \tag{3}$$

where a_0 is the amplitude,f_0 is the initial frequency, φ_0 is the initial phase, and $\mu_0 = B/T$ is the chirp rate with bandwidth B and duration time T.

The FrFT of $x(t)$ can be represented as

$$X(\alpha,u) = a_0 e^{j\varphi_0}\sqrt{\frac{1+j\tan\alpha}{1+\mu_0\tan\alpha}}\, e^{[j\pi\frac{u^2(\mu_0-\tan\alpha)+2uf_0\sec\alpha - f_0^2\tan\alpha}{1+\mu_0\tan\alpha}]}. \tag{4}$$

According to the rotation property of FrFT, the Wigner-Ville distribution (WVD) of FrFT of a signal with rotation angle α is the WVD of this signal rotated by a rotation angle $-\alpha$ [14]. In Fig. 1, as the angle rotates from the time domain, the fractional Fourier domain is defined as the dechirped domain when the axis u coincides with the energy bar of signal. Besides, the domain is perpendicular to the dechirped domain can be defined as the Energy-concentrated domain in which chirp signal acquires the best energy concentration property [14]. The rotation angles of

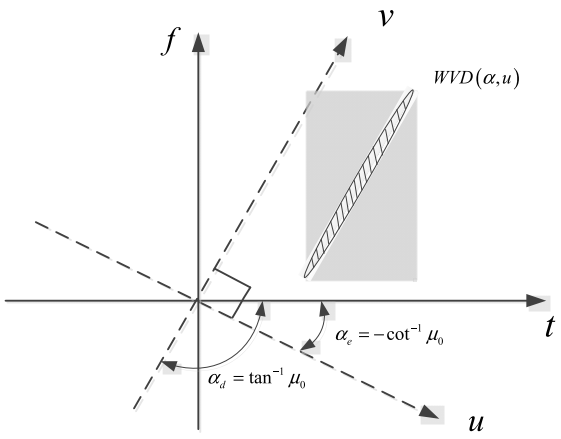

FIGURE 1. The energy spectrum of chirp signal in the time-frequency domain with the rotation angle α_e.

the dechirped domain and the Energy-concentrated domain of $x(t)$ are

$$\alpha_d = \operatorname{arctan}\ \mu_0, \tag{5}$$

$$\alpha_e = -\operatorname{arccot}\ \mu_0. \tag{6}$$

Obviously, according to the relationship between the rotation angle α_d and α_e, we can obtain that $\alpha_d = \alpha_e + \pi/2$.

According to the additivity of FrFT, we have

$$X(\alpha_d, u) = F[X(\alpha_e, u)], \tag{7}$$

which means that the FrFT of chirp signal in the dechirped domain equals to the FT of the FrFT of this signal in the Energy-concentrated domain.

In the dechirped domain, we have

$$X(\alpha_d, u) = B\exp(j2\pi f_0 \cos\alpha_d u), \tag{8}$$

where

$$B = a_0 \cos\alpha_d \sqrt{1 + j\tan\alpha_d} \times \exp\left[j\left(\varphi_0 - \pi f_0^2 \sin\alpha_d \cos\alpha_d\right)\right], \tag{9}$$

is a constant.

As indicated by the equations above, a chirp signal can be dechirped as a signal with single-frequency in the dechirped domain, that is

$$f_d = f_0 \cos\alpha_d. \tag{10}$$

In the Energy-concentrated domain, we have

$$X(\alpha_e, u) = C\delta(u\csc\alpha_e - f_0), \tag{11}$$

where

$$C = a_0\sqrt{-j - \cot\alpha_e}\exp\left[j\left(\varphi_0 + \pi/4\right)\right], \tag{12}$$

is a constant as well. In this domain, chirp signal acquires the highest energy concentration that is indicated by an impulse. The u coordinate of this impulse is

$$u_e = f_0 \sin\alpha_e. \tag{13}$$

In the following section, the coherently distributed source model and the steering vector for chirp signals in the dechirped domain will be reviewed.

III. DATA MODEL AND STEERING VECTOR

Consider the case of q distributed chirp sources in the far field impinging on an array with r sensors, where each sensor has the same gain, phase, and sensitivity pattern. The complex envelope of the output vector in the array can be modeled as [13]

$$\mathbf{y}(t) = \sum_{i=1}^{q} \int_{\vartheta\in\Theta} \mathbf{a}(\vartheta, t)\varsigma_i(\vartheta, \boldsymbol{\psi}_i; t)\, d\vartheta + \mathbf{n}(t), \tag{14}$$

where the steering vector $\mathbf{a}(\vartheta, t)$ of the array is time-varying, $\varsigma_i(\vartheta, \boldsymbol{\psi}_i; t)$ is the angular density of the ith chirp source in the direction $\vartheta \in \Theta$, $\boldsymbol{\psi}_i$ is the unknown location parameter vector of the ith chirp source including the central angle θ_i and the extension width Δ_i, and $\mathbf{n}(t)$ is an additive zero-mean noise vector. A number of N independent observations, $\mathbf{y}(1), \mathbf{y}(2), \ldots, \mathbf{y}(N)$, are collected by the array. Given these observations, we aim to estimate the location parameters of sources. Nevertheless, other unknowns usually exist in the parameter as well, such as initial frequency and chirp rate, which will seriously increase the complexity of estimation.

When the components at different angles from the same source can be regarded as the delayed and scaled replicas of the same signal, the source can be considered as a CD source [6]. For CD sources, the angle signal density can be represented by

$$\varsigma_i(\vartheta, \boldsymbol{\psi}_i; t) = s_i(t) \cdot \ell_i(\vartheta, \boldsymbol{\psi}_i), \tag{15}$$

where $s_i(t)$ is a random variable which reflects the temporal property of distributed source, while $\ell_i(\vartheta, \boldsymbol{\psi}_i)$ is the deterministic angular signal density which is a complex deterministic function of ϑ.

In this paper, the vector of signal waveforms $\mathbf{s}(t)$ is assumed to be a zero-mean, temporally complex Gaussian distributed random variable.

For CD sources, the FrFT of (14) can be expressed as

$$\mathbf{Y}(\alpha, u) = \sum_{i=1}^{q} \int_{\vartheta\in\Theta} \mathbf{A}(\alpha, \vartheta; u) S_i(\alpha, u)\ell_i(\vartheta, \boldsymbol{\psi}_i)\, d\vartheta + \mathbf{N}(\alpha, u) \tag{16}$$

where $S_i(\alpha, u)$ is the FrFT of $s_i(t)$, $\mathbf{N}(\alpha, u)$ is the FrFT of $\mathbf{n}(t)$, and $\mathbf{A}(\alpha, \vartheta; u)$ is the steering vector in the fractional Fourier domain.

Let $\mathbf{b}(\alpha, \boldsymbol{\psi}_i; u)$ be defined as

$$\mathbf{b}(\alpha, \boldsymbol{\psi}_i; u) = \int_{\vartheta\in\Theta} \mathbf{A}(\alpha, \vartheta; u)\ell_i(\vartheta, \boldsymbol{\psi}_i)\, d\vartheta. \tag{17}$$

For a uniform linear array (ULA), the steering vector on the kth sensor in the dechirped domain can be given by [13]

$$A_k(\alpha_d, \theta) = e^{j\pi\left[(\tau_k)^2 \sin\alpha_d \cos\alpha_d - 2f_0 \cos^2\alpha_d \tau_k\right]}, \tag{18}$$

where $\tau_k = (k-1)d\sin(\theta)/c$ represents the time delay which performs on the kth sensor, d is the distance between two adjacent sensors in the array, θ is the incident angle of the signal and c is the speed of signal propagation.

Finally, the steering vector can be written as

$$\mathbf{A}(\alpha_d, \theta) = [1, A_2(\alpha_d, \theta), \cdots, A_r(\alpha_d, \theta)]^{\mathrm{T}}. \tag{19}$$

In the dechirped domain, the influence of the time variable and the variable u in the steering vector are eliminated. Then, (18) in the dechirped domain can be written as

$$\mathbf{Y}(\alpha_d, u) = \sum_{i=1}^{q} \mathbf{b}(\alpha_d, \boldsymbol{\psi}_i) S_i(\alpha_d, u) + \mathbf{N}(\alpha_d, u), \tag{20}$$

where

$$\mathbf{b}(\alpha_d, \boldsymbol{\psi}_i) = \int_{\vartheta \in \Theta}^{\mathbf{A}(\alpha_d, \vartheta)\ell_i(\vartheta, \boldsymbol{\psi}_i)} d\vartheta. \tag{21}$$

For the array $\mathbf{Y}$, the covariance matrix in the dechirped domain is given by

$$\begin{aligned}\mathbf{R_{YY}} &= \sum_{i=1}^{q}\sum_{j=1}^{q} \mathbf{b}(\alpha_d, \boldsymbol{\psi}_i) E\{S_i(\alpha_d, u) S_j^H \\ &\quad \times (\alpha_d, u)\}\mathbf{b}^H(\alpha_d, \boldsymbol{\psi}_j) + \mathbf{R_{NN}} \\ &= \mathbf{B}(\alpha_d, \boldsymbol{\psi}) \boldsymbol{P} \boldsymbol{B}^H(\alpha_d, \boldsymbol{\psi})\, \boldsymbol{\mathcal{C}}\, \boldsymbol{R}_{\mathbf{NN}}\end{aligned} \tag{22}$$

where

$$\mathbf{B}(\alpha_d, \boldsymbol{\psi}) = \left[\mathbf{b}(\alpha_d, \boldsymbol{\psi}_1)\ \ \mathbf{b}(\alpha_d, \boldsymbol{\psi}_2) \cdots \mathbf{b}(\alpha_d, \boldsymbol{\psi}_q)\right], \tag{23}$$

$$[\mathbf{P}]_{ij} = E\left\{S_i(\alpha_d, u) S_j^H(\alpha_d, u)\right\}, \tag{24}$$

$$\mathbf{R_{NN}} = \sigma_n^2 \mathbf{I}, \tag{25}$$

and σ_n^2 is the noise variance. Notice that the statistical characteristic of random signals is not affected by the FrFT (see Appendix A).

Performing the eigendecomposition on $\mathbf{R_{YY}}$ renders

$$\mathbf{R_{YY}} = \boldsymbol{U}_S \boldsymbol{\Sigma}_S \boldsymbol{U}_S^H + \boldsymbol{U}_N \boldsymbol{\Sigma}_N \boldsymbol{U}_N^H, \tag{26}$$

where the column vectors of $\boldsymbol{U}_S$ and $\boldsymbol{U}_N$ respectively are the eigenvectors that span the signal subspace and the noise subspace of $\mathbf{R_{YY}}$ with the associated eigenvalues on the matrixes of $\boldsymbol{\Sigma}_S$ and $\boldsymbol{\Sigma}_N$.

Hence, (20) can be rewritten as

$$\mathbf{Y}(\alpha_d, u) = \mathbf{B}(\alpha_d, \boldsymbol{\psi})\mathbf{S}(\alpha_d, u) + \mathbf{N}(\alpha_d, u), \tag{27}$$

where

$$\mathbf{S}(\alpha_d, u) = \left[S_1(\alpha_d, u)\ \ S_2(\alpha_d, u)\ \ \cdots\ \ S_q(\alpha_d, u)\right]^T. \tag{28}$$

Based on these analyses, a novel low-complexity MUSIC- type estimator of the spatial parameters for multiple sources will be proposed in the next section.

IV. SPATIAL PARAMETER ESTIMATION

The excessive computational complexity, which needs to carry out complicated searches over unknown parameters in multidimensional spaces, is one of the major disadvantages of traditional distributed source estimators. To address this problem, we propose a method that combines the frequency parameter estimation with a two-step 1D MUSIC over reduced dimension parameter search spaces.

A. DIMENSION REDUCTION

We will discuss the case of one distributed chirp source (i.e. $q = 1$ in (14)) first. The unknown model parameters $\boldsymbol{\eta}$ in the estimate can be given by

$$\boldsymbol{\eta} = \left[\boldsymbol{\psi}^T, \boldsymbol{w}^T\right]^T, \tag{29}$$

where $\boldsymbol{\psi} = [\theta_1\ \Delta_1]^T$ is the spatial parameter vector, and $\boldsymbol{w} = [f_1\ \mu_1]^T$ is the frequency parameter vector.

As we can see from (29), the parameter estimation algorithm for a distributed chirp source model requires a high-dimensional optimization which causes substantial computational complexity. To address this issue, we try to reduce dimension parameter search spaces through estimating the frequency parameter which is easily obtained by (6) and (13) in the Energy-concentrated domain. The estimation results also can be written as

$$\begin{cases} \hat{f}_0 = \hat{u}_e \csc \hat{\alpha}_e \\ \hat{\mu}_0 = -\cot \hat{\alpha}_e. \end{cases} \tag{30}$$

The observed signal is processed with a continuously varying rotation angle α, and the estimation $(\hat{\alpha}_e, \hat{u}_e)$ can be determined by finding the coordinate of spectrum peak in the fractional Fourier domain.

Since the frequency parameters can be estimated previously, the number of the unknown parameters in (29) is reduced and then $\boldsymbol{\eta}$ can be reformed as

$$\boldsymbol{\eta}' = [\boldsymbol{\psi}]. \tag{31}$$

Then, the MUSIC-type estimate of the unknown parameter $\boldsymbol{\psi}$ can be easily extended to the proposed model. Then, we have

$$\hat{\boldsymbol{\psi}} = \arg\max_{\boldsymbol{\psi}} \frac{\mathbf{B}^H\mathbf{B}}{\mathbf{B}^H \boldsymbol{\Pi}_n \mathbf{B}}, \tag{32}$$

where $\boldsymbol{\Pi}_N = \boldsymbol{U}_N \boldsymbol{U}_N^H$. This estimator needs to carry out a 2D search over the parameter $\boldsymbol{\psi}$ using (32).

B. TWO-STEP 1D MUSIC

To further reduce the computational complexity of the proposed approach, we present a lower cost strategy in this part. According to the measurement results of [17] and [18], depending on the environment of the mobile, the base-mobile distance and the base station height, the extension width less than 6^{o} can be commonly observed in practice.

Thus, considering $\vartheta \in \Theta$ in (17) is small, the steering vector $\mathbf{B}$ can be factorized as (see Appendix B)

$$\mathbf{B} = \mathbf{A} \odot \mathbf{G}. \tag{33}$$

Inserting (33) into the expression of MUSIC estimator (32) yields

$$\hat{\boldsymbol{\psi}} = \arg\max_{\boldsymbol{\psi}} \frac{\mathbf{G}^H \odot \mathbf{A}^H \mathbf{A} \odot \mathbf{G}}{\mathbf{G}^H \odot \mathbf{A}^H \boldsymbol{\Pi}_n \mathbf{A} \odot \mathbf{G}}, \tag{34}$$

It should be noted that there exists a matrix $\bar{\mathbf{G}}$ satisfying $\bar{\mathbf{G}} \odot \mathbf{G} = \mathbf{1}$ where $\mathbf{1}$ is a matrix with all entries are 1. Then, (33) can be simplified as

$$\hat{\theta} = \arg\max_{\theta} \frac{\mathbf{A}^H \mathbf{A}}{\mathbf{A}^H \boldsymbol{\Pi}_n \mathbf{A}}. \tag{35}$$

The maximization of (35) can be performed using the 1D search over the central angle. After that, substituting the estimated central angle into (32), the extension width can be obtained by the second step 1D MUSIC. Note that the estimation of central angle does not rely on any assumption of deterministic angular signal densities and should be robust to mismodeling $\ell(\vartheta, \boldsymbol{\psi})$.

The main idea of the EXIP is to reparameterize the estimating criterion in terms of a less detailed parameter vector with a view to facilitate solving the minimization problem [10]. Based on the EXIP, the convergence will be discussed as follow.

Maximizing (32) is equivalent to minimizing

$$\begin{aligned} V(\boldsymbol{\psi}) &= \mathbf{B}^H \boldsymbol{\Pi}_n \mathbf{B} \\ &= (\mathbf{A} \odot \mathbf{G})^H \boldsymbol{\Pi}_n (\mathbf{A} \odot \mathbf{G}) \\ &= \mathbf{A}^H \boldsymbol{\Pi}_n \mathbf{A} \odot \mathbf{G}^H \mathbf{G} \end{aligned} \tag{36}$$

Let $\gamma = \mathbf{G}^H \mathbf{G}$. Differentiating (36) with respect to γ, we obtain

$$\frac{\partial V(\boldsymbol{\psi})}{\partial \gamma} = \mathbf{A}^H \Pi_n \mathbf{A} \tag{37}$$

Theoretically, the variable γ can minimize (36), only when $\mathbf{A}^H \boldsymbol{\Pi}_n \mathbf{A} = 0$ (i.e., the maximization of (35)) is satisfied. Hence, the two spatial parameter estimation ensures the convergence.

C. MULTIPLE SOURCES ESTIMATION ALGORITHM

1) SEPARABLE CASES

According to (11) and (13), we know that chirp signals with different initial frequencies or chirp rates have different support positions in the fractional Fourier domain, which ensures that the signals are separable. Fig. 2 shows the spectrum distributions of the two chirp signals with different initial frequencies and different chirp rates in the fractional Fourier domain. As mentioned in section II, the energy distribution of each chirp source in its Energy-concentrated domain shows a distinct spectral peak, while that of other signals with different chirp rates and noise is dispersing in this domain.

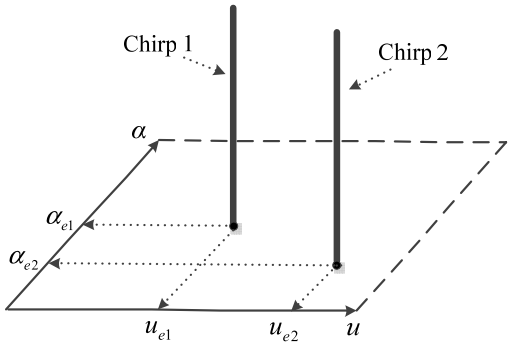

FIGURE 2. The spectrum distributions of chirp signals in the fractional Fourier domain.

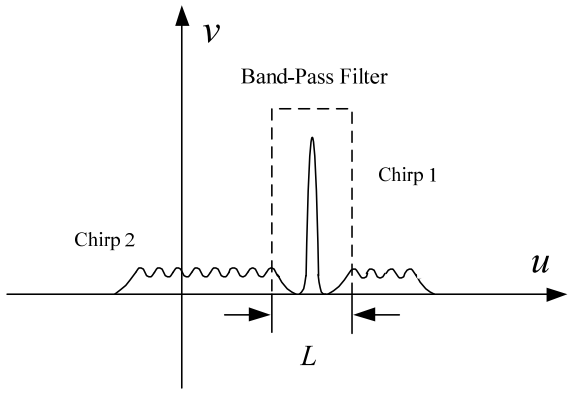

FIGURE 3. The spectrum distributions of chirp signals in the Energy-concentrated domain.

Therefore, multiple chirp sources can be conveniently separated in their own Energy-concentrated domain by applying a band-pass filter, as shown in Fig. 3.

After the filtered signal is transformed into the dechirped domain by the FT, the aforementioned method for single source can be applied. Finally, by repeating the above steps, the desired parameters of all distributed chirp sources can be obtained respectively.

When q chirp sources all have different frequency parameters, the steps used for the proposed estimator in the separable cases are carried out by the following steps.

In the frequency parameter estimation (step 1 to 3), the iterative search based on quasi-Newton method proposed in [19] can observably reduce the computation complexity of 2D search in the (α, u) plane. The computation complexity of this iterative method is $O(mN \log N)$, where m is the number of the steps in the scanning, which is likely to be much less than N when the resolution and the range are selected properly. Then, α_d can be acquired by the relationship between α_d and α_e in (7). And the filter processing (step 4) costs $O(N)$ to find the peak and filter.

Since the operation of complex multiplication is the major computation when estimating spatial parameter, we mainly consider that cost in step 5 and step 6. The eigen-decomposition needs $O\left(Nr^2 + r^3\right)$. Solving $\boldsymbol{\Pi}_n$ costs $O\left(r^2 (r - q)\right)$. In the proposed estimator, the

Algorithm 1 Estimation of Spatial Parameters of Separable Sources

Step 1: Search over parameters (α, u) is performed on the received signals of the first sensor by the FrFT.
Step 2: Estimate $\left\{\hat{\alpha}_{ei}, \hat{u}_{ei}\right\}_{i=1}^{q}$ by peak searching of the energy spectrum in the (α, u) plane.
Step 3: Estimate $\left\{\hat{f}_{ei}, \hat{\mu}_{ei}\right\}_{i=1}^{q}$ based on (30).
for $i = 1 : q$ do
  Step 4: Obtain the filtered signal $s_i(t)$ on each sensor by the filter processing in its Energy-concentrated domain.
  Step 5: Estimate $\hat{\theta}_i$ from (35) in the dechirped domain of $s_i(t)$.
  Step 6: Estimate $\hat{\Delta}_i$ from (32) with $\theta = \hat{\theta}_i$.
end for

1D spectral search for the central angle and the extension width require $O\left(\bar{m}\left(r^2+2r\right)\right)$ and $O\left(\bar{n}\left(r^2+2r\right)\right)$, where $\bar{m}$ and $\bar{n}$ are the number of the steps in the scanning for the central angle and the extension width respectively. Thus, the complexity of estimating spatial parameter is $O\left(r^2(r-q)+\bar{m}\left(r^2+2r\right)+\bar{n}\left(r^2+2r\right)\right)$, while the 2D searches within the method in [13] requires $O\left(r^2(r-q)+\bar{m}\bar{n}\left(r^2+2r\right)\right)$. The two spatial parameters can be simply acquired by a two-step 1D MUSIC algorithm which dramatically decreases the computational complexity. The refinement method can also be exploited in our proposed method. A coarse search is performed firstly, and then we get a refined grid around the location of the peak acquired at the first step. This refinement process is repeated until the location of the peak is found. In our simulations, the uniform sampling grid is utilized. To avoid introducing substantial bias, the sampling interval of the first step is set to 1°.

2) INSEPARABLE CASES

While chirp signals possess the same frequency parameters, they share the same peak position in the fractional Fourier domain and cannot be separated from each other. These signals possess the same dechirped domain with the same rotation angle. This case can be simply considered as a classical DOA estimation problem of multiple signals, since all the sources share the same manifold in that domain. The central angles of sources with the same frequency parameters can be simultaneously estimated by (35) in the same dechirped domain. After that, each extension width can be obtained by (32) respectively.

Assume q chirp source groups have q different frequency parameters and the ith source group contains $\{L_i\}_{i=1}^{q}$ sources sharing the same frequency parameter. That means the $\{L_i\}_{i=1}^{q}$ $(L_i < r)$ sources in the ith source group have the same chirp rate and the same dechirped domain. In this case, the major steps of the proposed algorithm are summarized as follows:

Algorithm 2 Estimation of Spatial Parameters of Inseparable Sources

Step 1: Search over parameters (α, u) is performed on the received signals of the first sensor by the FrFT.
Step 2: Estimate $\left\{\hat{\alpha}_{ei}, \hat{u}_{ei}\right\}_{i=1}^{q}$ by peak searching of the energy spectrum in the (α, u) plane.
Step 3: Estimate $\left\{\hat{f}_{ei}, \hat{\mu}_{ei}\right\}_{i=1}^{q}$ based on (30).
for $i = 1 : q$ do
  Step 4: Obtain the filtered ith source group on each sensor by the filter processing in its Energy-concentrated domain.
  Step 5: Estimate $\left\{\hat{\theta}_{ik}\right\}_{k=1}^{L_i}$ from (35) in the dechirped domain of the ith source group.
  for $k = 1 : L_i$ do
    Step 6: Estimate $\hat{\Delta}_{ik}$ from (32) with $\theta = \hat{\theta}_{ik}$.
  end for
end for

In the proposed algorithm, the deterministic angular signal densities of incident sources can be different, because the extension width of each source is independently estimated by (32). Furthermore, a Toeplitz matrix is applied to remove the coherency when chirp signals are coherent, and then (22) can be transformed into

$$\mathbf{R_{YY}} = \begin{bmatrix} R_{11} & R_{12} & \cdots & R_{1r} \\ R_{12}^{*} & R_{11} & \cdots & R_{1(r-1)} \\ \vdots & \vdots & \ddots & \vdots \\ R_{1r}^{*} & R_{1(r-1)}^{*} & \cdots & R_{11} \end{bmatrix}_{r\times r} \tag{38}$$

3) CRB IN THE DECHIRPED DOMAIN

CRB serves as a well-known benchmark for the variance of unbiased estimators in signal processing. Generally, two main types of the DOA's CRB of the received signal are studied: deterministic and stochastic. In this paper, the received signal in the model can be interpreted as multiple Gaussian stochastic signals with certain angle spread. Hence, we will focus on the stochastic CRB study. In previous works, the stochastic CRB for the DOA estimation of narrowband signals in array processing is indirectly derived as the (asymptotic) covariance matrix of the ML estimator in [20] and [21]. Stoica *et al.* [22] provide a standard form for calculating the stochastic CRB. According to the analysis in Section II. B, those conclusions can be easily extended to the model in this paper. Then, in the dechirped domain, we obtain

$$\mathrm{CRB}(\boldsymbol{\psi}) = \frac{\sigma_n^2}{2N}\left\{\mathrm{Re}\left[\mathbf{H}\odot\left(\mathbf{P}\mathbf{B}^H\mathbf{R}_{\mathbf{XX}}^{-1}\mathbf{B}\mathbf{P}\right)^T\right]\right\}^{-1}, \tag{39}$$

where

$$\mathbf{H} = \mathbf{D}^H\left[\mathbf{I}-\mathbf{B}\left(\mathbf{B}^H\mathbf{B}\right)^{-1}\mathbf{B}^H\right]\mathbf{D}, \tag{40}$$

$$\mathbf{D} = [\mathbf{d}_1\ \cdots\ \mathbf{d}_r], \tag{41}$$

and

$$\boldsymbol{d}_i = d\mathbf{B} \Big/ d\boldsymbol{\psi}|_{\boldsymbol{\psi}=\boldsymbol{\psi}_i}. \tag{42}$$

Notice that, there are four variables in the CRB representation in (39). Therefore, the exact determination of the CRB cannot be done directly. To evaluate the performance of proposed algorithm by the CRB in the simulation, except for the desired variable, the other three are assumed to be known during the whole observation time. Then, the CRB of desired variable can be obtained under this assumption, which is referred as the essential benchmark of the proposed algorithm.

V. SIMULATION STUDY & RESULTS

A. DIGITAL CALCULATION OF THE FrFT

In our simulation, we employ the fast implementation of the digital calculation of FrFT based on the fast Fourier transform (FFT) [23], which has a lower complexity of $O(N \log N)$ and high accuracy.

Because the chirp signal cannot be compact both in the time and frequency domain, the energy of signal may be out of the valid domain with the rotation of the FrFT. To solve this problem, Liu *et al.* [24] published details of the dimensional normalization processing when dealing with discrete signals in the fractional Fourier domain. Let the chirp signal in the time domain be confined to the interval $[-\Delta T/2,\ \Delta T/2]$ and its frequency domain representation be confined to the interval $[-\Delta F/2,\ \Delta F/2]$. Under this assumption, most of the signal energy is confined to these intervals. To satisfy the requirement that the time and frequency domain are compact at the same time, the scaling parameter $\kappa = \sqrt{\Delta T/\Delta F}$ is introduced. The time domain and the frequency domain representations are confined to intervals of length $\Delta T/\kappa$ and $\Delta F\kappa$ respectively. Thus, the lengths of both intervals become the dimensionless quantity $\sqrt{\Delta T\,\Delta F}$, while the sample interval satisfies that $\Delta x = \sqrt{N} = 1\Big/\sqrt{\Delta T\,\Delta F}$, which is scaled to 1 for simplicity. We assume that ΔT is the duration time T and ΔF is the sample frequency f_s. By employing the dimensional normalization processing, the representations of $(\alpha_e,\ u_e)$ can be restated as

$$\begin{cases} \tilde{\alpha}_e = -\text{arc}\cot(\mu_0 N/f_s^2) \\ \tilde{u}_e = f_0 N \sin\tilde{\alpha}_e/f_s. \end{cases} \tag{43}$$

B. SIMULATION SETUP

In the simulation, a ULA of $r = 8$ sensors is considered. The deterministic angular signal densities of two coherently Gaussian-distribution linear chirp sources, are defined as

$$\ell(\vartheta, \boldsymbol{\psi}) = \frac{1}{\sqrt{2\pi}\,\Delta_i} \exp\left(-\frac{(\vartheta-\theta_i)^2}{2\Delta_i^2}\right)\Bigg|_{i=1,2}, \tag{44}$$

while the signal-to-noise ratio is defined as

$$\text{SNR} = 10\log\frac{E\left[|s(t)|^2\right]}{T\sigma_n^2}. \tag{45}$$

TABLE 2. The parameters of signals in simulations.

Parameter	Value
Initial frequency	$f_1 = 100\text{MHz}$, $f_2 = 300\text{MHz}$
Chirp rate	$\mu_1 = 10\times10^{12}\,\text{Hz/s}$, $\mu_2 = -80\times10^{12}\,\text{Hz/s}$
The central angle	$\theta_1 = 30^\circ$, $\theta_2 = 60^\circ$
The extension width	$\Delta_1 = 2^\circ$, $\Delta_2 = 3^\circ$
Sample number	$N = 301$
SNR	$\text{SNR} = 10\text{dB}$

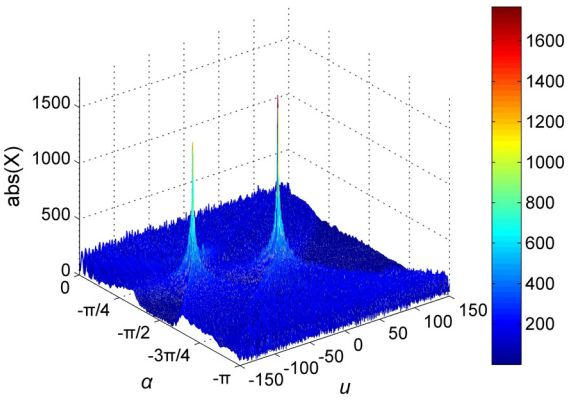

FIGURE 4. The energy spectra of tested chirp sources in the (α, u) plane.

Monte Carlo simulations of 1000 independent runs are performed for each simulation. The method proposed in [13], which is a generalized DSPE for distributed chirp source, is chosen as the benchmark algorithm for estimating the central angle and the extension width of the incident source. The parameters of two received signals in these simulations are summarized in Table 2.

C. RESULTS AND ANALYSIS

1) FREQUENCY PARAMETER ESTIMATION AND FILTERING PROCESS

In the following part, we focus on studying the source one for conciseness, and stress that the similar conclusion can be easily extended to the source two. The spectrum of the both sources in the (α, u) plane is shown in Fig. 4. The true values $(\tilde{\alpha}_{e1}, \tilde{u}_{e1})$ and the estimation values $(\hat{\alpha}_{e1}, \hat{u}_{e1})$ are presented respectively as follow:

$$\begin{cases} \tilde{\alpha}_{e1} = -1.5374 \\ \tilde{u}_{e1} = -100.2774, \end{cases} \tag{46}$$

$$\begin{cases} \hat{\alpha}_{e1} = -1.5367 \\ \hat{u}_{e1} = -100. \end{cases} \tag{47}$$

As illustrated in Fig. 5(a), the energy spectrum of tested chirp signal one without noise on the first sensor in the

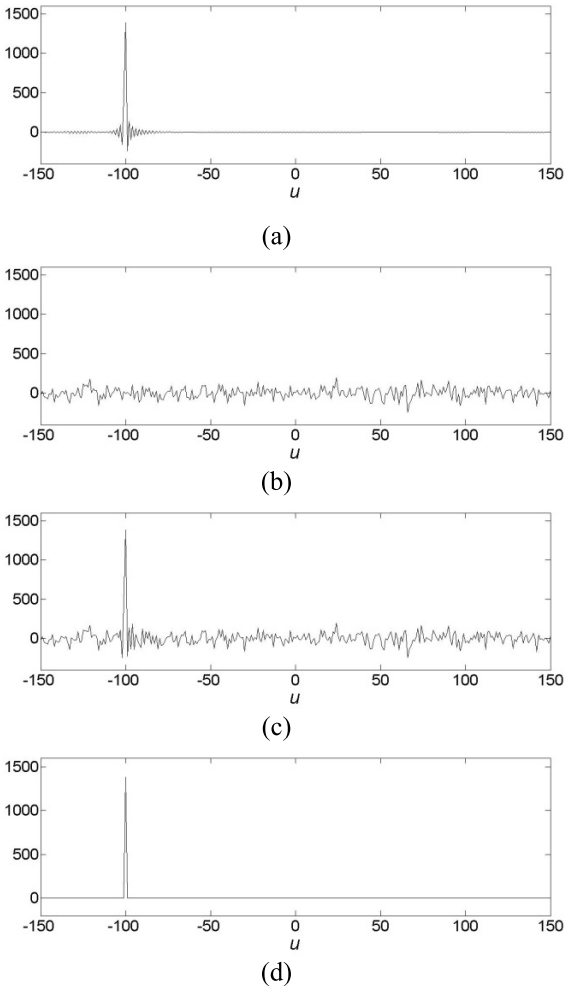

FIGURE 5. The energy spectrum of chirp signal and noise on the first sensor in the Energy-concentrated domain. (a) tested chirp signal one without noise (b) noise (c) tested chirp signal with noise (d) filtered signal.

Energy-concentrated domain shows an obvious energy concentration around $\hat{u}_{e1}$. In this Energy-concentrated domain, the chirp signal forms a sinc function and the majority of energy spectrum focuses on its support. The energy spectrum of noise and other signals is relatively lower and more dispersed, which affects the support of chirp signal slightly, as shown in Fig. 5(b) and (c). Similarly, the single spectrum peak will appear on the other sensors as well. Therefore, the desired chirp signal can be separated from the other signals and the noise.

For selecting a bandwidth L of the band-pass filtering, we must estimate the width of chirp signal's support in the Energy-concentrated domain using [24]

$$\rho_\alpha = \left|\Delta x \left(\cos\alpha + \mu_1 \Delta T / \Delta f \sin\alpha\right)\right|. \tag{48}$$

According to (48), we know that $\rho_{\alpha=\alpha_{e1}}$ can be easily obtained based on the estimation results in (43) and (48). The simplest selection method is that the bandwidth L is rounded up to the integer value of ρ_α, which ensures that the majority

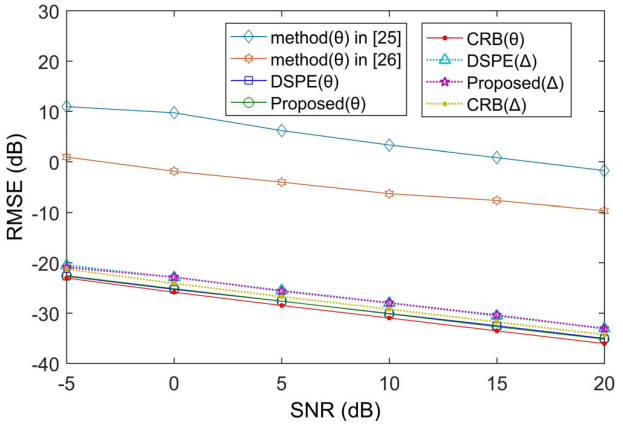

FIGURE 6. RMSEs for the central angle and the extension width estimates versus SNRs.

of energy of the signal is reserved while that of the noise and other signals is eliminated. Using a rectangular window with the bandwidth L, the filtered signal is presented in Fig. 5(d).

2) LOCATION PARAMETERS ESTIMATION FOR SOURCE ONE

Next, we study the estimation performance of unknown location parameters for the proposed method and the generalized DSPE when different parameters in Table 2 are varied one at a time. The methods in [25] and [26], which are proposed to estimate the DOA of chirp signals based on the point source model, are also chosen as the comparisons to demonstrate that the proposed algorithm has better performance when estimating distributed sources. The simulation results of source one are shown in following parts.

The simulation is carried out in a range of SNR values. The root-mean square error (RMSE) for the central angle and the extension width estimates versus different SNRs are shown in Fig. 6. As we can see, the proposed method provides similar performance to the DSPE on the central angle and the extension width estimation versus different SNRs. The empirical results of the proposed method and the generalized DSPE are close to the CRB in the distributed source condition.

The influence of extension widths on the performance can be observed in Fig. 7. When the extension width is smaller than 5°, the proposed estimator has similar performance to the DSPE. As the extension width increases, the RMSEs for the central angle estimates of the proposed estimator increase faster than the DSPE. The main reason is that the approximations of (B3) and (B4) introduce more bias with the increase of the extension width. Since the proposed estimator in (35) is based on this approximation, the estimation accuracy deteriorates with the extension width increasing.

The influence of sample number and sensor number are presented in Fig. 8 and Fig. 9, respectively. The proposed estimator performs very close simulation results to the DSPE for small extension width. When sample number or sensor

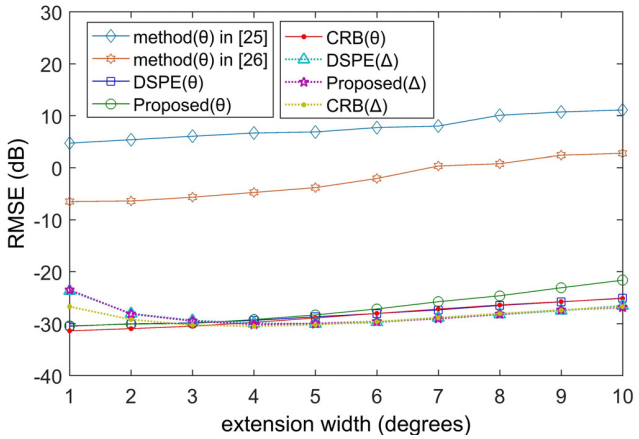

FIGURE 7. RMSEs for the central angle and the extension width estimates versus extension widths.

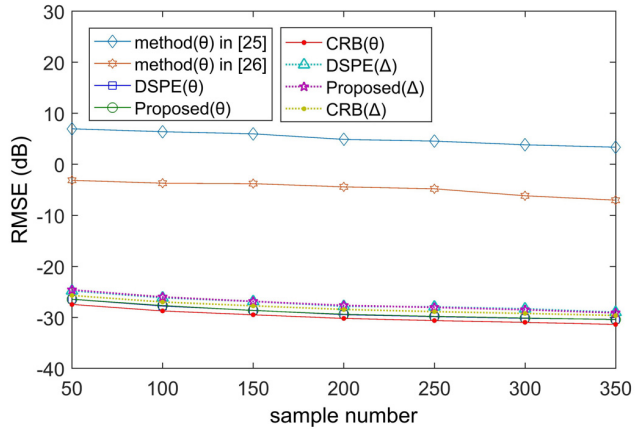

FIGURE 8. RMSEs for the central angle and the extension width estimates versus sample numbers.

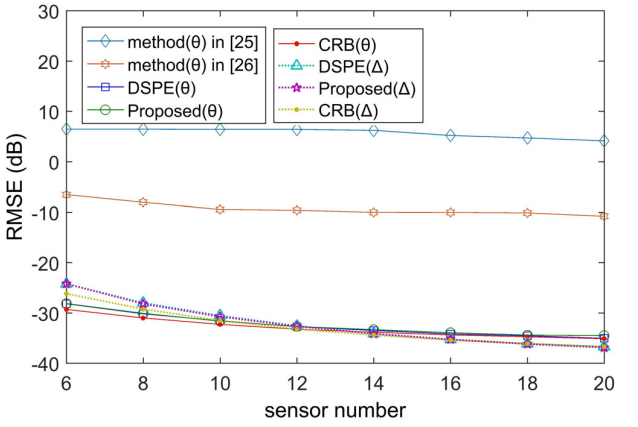

FIGURE 9. RMSEs for the central angle and the extension width estimates versus sensor numbers.

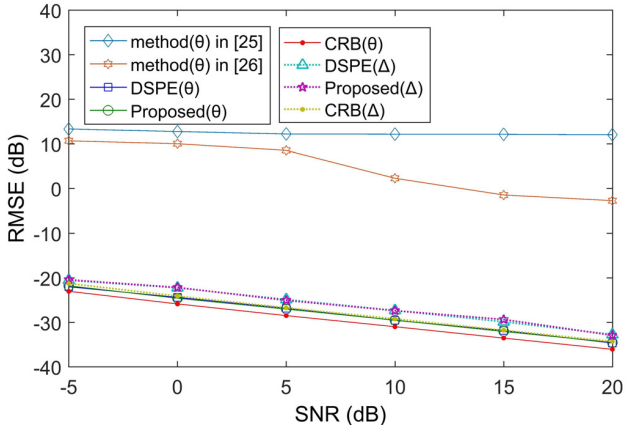

FIGURE 10. RMSEs for the central angle and the extension width estimates versus SNRs in the case of coherent and inseparable sources.

number increases, the estimation performance improves. The estimations of location parameters are similarly affected by the increase of sample number. While the sensor number is large enough, the estimation of extension width is better than that of central angle. The estimation performance of location parameters for the two estimators are closer to the CRB as sensor number increases.

We consider the coherent and the inseparable sources scenarios in the following test. The source two has the same frequency parameters as the source one and their correlation coefficient is set to 1. The two sources cannot be separated in this case. The covariance matrix is reconstructed as the Toeplitz matrix (38) which removes the coherency. The results for source one are shown in Fig. 10. The proposed estimator remains similar performance with the DSPE.

As we can see from the results in this section, the estimators [25], [26] based on the point source assumption cannot work well to estimate distributed chirp sources, while the proposed algorithm has the similar performance to the DSPE and the CRB.

3) LOCATION PARAMETERS ESTIMATION FOR MULTIPLE SOURCES

Finally, we demonstrate the resolution performance of the proposed algorithm versus different source number. In this experiment, all sources have the same initial frequencies, and three different chirp rate intervals are tested. The SNR is 0dB. The RMSE of the estimated central angle using the proposed algorithm is shown in Fig. 11. The proposed algorithm contains filter and separation process which reduces the interference caused by noise and other interference signals. However, the finite duration chirp signal in its Energy-concentrated domain is not a simple Dirac delta function but a sinc function. The separation performance and the rotation angle determination of Energy-concentrated domain will be seriously affected as the growth of source number because of the interference of superposed signal energy. A larger chirp rate interval can decrease this bidirectional interference effectively, since it provides a longer distance between two supports in the fractional Fourier domain. Therefore, the good resolution performance of the proposed estimator can be maintained if the frequency parameter

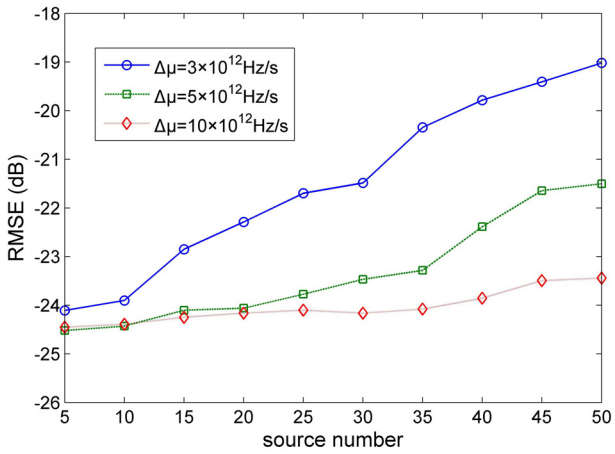

FIGURE 11. RMSEs for the central angle versus different source numbers.

interval of each source is large enough and the source number is not too many.

VI. CONCLUSION

In this paper, we considered the problem of the parametric localization of multiple coherently distributed linear chirp sources. A novel low-complexity MUSIC-type estimator of source parameters and the corresponding CRB in the dechirped domain were proposed. By using the properties of chirp signals in the fractional Fourier domain, the frequency parameters can be acquired firstly. After that, a two-step 1D MUSIC method was applied to estimate the spatial parameters of sources. Numerical results demonstrated that the proposed method provided an acceptable spatial resolution performance for distributed linear chirp source with significantly decreased complexity for small extension width.

APPENDIX

A. THE STATISTICAL PROPERTY OF RANDOM SIGNAL IN THE FRACTIONAL FOURIER DOMAIN

In this section, we demonstrate that the statistical property of signals will not be affected after applying the FrFT with any rotation angle.

Firstly, three significant properties of the FrFT used in our demonstration are as follow:

$$(F^p)^{-1} = (F^p)^H, \tag{A1}$$
$$(F^p)^{-1} = F^{-p}, \tag{A2}$$
$$F^{p_1}F^{p_2} = F^{p_1+p_2}, \tag{A3}$$

and we assume that

$$E\left\{\boldsymbol{s}(t_i)\boldsymbol{s}^H(t_j)\right\} = \mathbf{P}_{ij}, \tag{A4}$$
$$E\left\{\boldsymbol{s}(t_i)\boldsymbol{s}^T(t_j)\right\} = \mathbf{Q}_{ij} \quad (\text{for all}\mathbf{t}_i \text{ and } \mathbf{t}_j). \tag{A5}$$

When the FrFT with the rotation angle α performed on the signal $\boldsymbol{s}(t)$, the equation (A4) in the fraction Fourier domain can be written as

$$\begin{aligned}
&E\left\{F^\alpha\left[\boldsymbol{s}(t_i)\right]\left(F^\alpha\left[\boldsymbol{s}(t_j)\right]\right)^H\right\} \\
&= E\left[\int_{-T/2}^{T/2}\sqrt{1-j\cot\alpha}\,e^{j\pi\left(t_1^2\cot\alpha-2t_iu\csc\alpha+u^2\cot\alpha\right)}\boldsymbol{s}\left(t_i\right)dt_i\right. \\
&\quad\left.\times\int_{-T/2}^{T/2}\sqrt{1+j\cot\alpha}\,e^{j\pi\left(-t_2^2\cot\alpha+2t_ju\csc\alpha-u^2\cot\alpha\right)}\boldsymbol{s}^H\left(t_j\right)dt_j\right] \\
&= E\left[\sqrt{1+\cot^2\alpha}\int_{-T/2}^{T/2}dt_i\right. \\
&\quad\left.\times\int_{-T/2}^{T/2}e^{j\pi\left(t_i^2-t_j^2\right)\cot\alpha}e^{-j2\pi\left(t_i-t_j\right)u\csc\alpha}\boldsymbol{s}\left(t_i\right)\boldsymbol{s}^H\left(t_j\right)dt_j\right]
\end{aligned} \tag{A6}$$

Then, we assume that $t_i - t_j = \tau$, such that

$$\begin{aligned}
&E\left\{F^\alpha\left[\boldsymbol{s}(t_i)\right]\left(F^\alpha\left[\boldsymbol{s}(t_j)\right]\right)^H\right\} \\
&= \sqrt{1+\cot^2\alpha}\int_{-T/2-t_j}^{T/2-t_j}d\tau \\
&\quad\times\int_{-T/2}^{T/2}e^{j\pi\left(2t_j+\tau\right)\tau\cot\alpha}e^{-j2\pi\tau u\csc\alpha}E\left[\boldsymbol{s}(t_j+\tau)\boldsymbol{s}^H(t_j)\right]dt_j \\
&= \mathbf{P}_{ij}\sqrt{1+\cot^2\alpha}\int_{-T/2-t_j}^{T/2-t_j}d\tau \\
&\quad\times\int_{-T/2}^{T/2}e^{j\pi\left(2t_j+\tau\right)\tau\cot\alpha}e^{-j2\pi\tau u\csc\alpha}dt_j \\
&= \mathbf{P}_{ij}F^\alpha\left(1\right)F^{-\alpha}\left(1\right) \\
&= \mathbf{P}_{ij}
\end{aligned} \tag{A7}$$

Similarly, we can easily get that

$$E\left\{F^\alpha\left[\boldsymbol{s}(t_i)\right]\left(F^\alpha\left[\boldsymbol{s}(t_j)\right]\right)^T\right\} = \mathbf{Q}_{ij}. \tag{A8}$$

As a result, the 2-order statistical properties of signals are not affected by the FrFT.

B. THE STEERING VECTOR FACTORIZING

In the dechirped domain, the steering vector on the kth sensor for the ith signal is

$$b_k = \int_{\vartheta\in\Theta}A_k(\alpha_d,\vartheta)\ell_i(\vartheta,\boldsymbol{\psi}_i)\,d\vartheta. \tag{B1}$$

Since Θ depends on the extension width Δ_i that is small in most scenarios, we assume that $\vartheta - \theta_i = \bar{\vartheta}$ and the value of $\bar{\vartheta}$ is small. (B.1) can be reconstructed by the above term as

$$b_k = \int_{\bar{\vartheta}\in\bar{\Theta}}A_k(\alpha_d,\theta_i+\bar{\vartheta})\ell_i(\theta_i+\bar{\vartheta},\boldsymbol{\psi}_i)\,d\bar{\vartheta}. \tag{B2}$$

Considering $\bar{\vartheta}$ is a small number, the term $\sin(\theta_i+\bar{\vartheta})$ can be approximated by using the first-order Taylor Series expansion, that is

$$\sin(\theta_i+\bar{\vartheta}) \cong \sin\left(\theta_i\right)+\bar{\vartheta}\cos\left(\bar{\vartheta}\right). \tag{B3}$$

Then, the term $A_k(\alpha_d,\theta_i+\bar{\vartheta})$ in (B2) can be approximated as (B4), shown at the top of the next page.

$$
\begin{aligned}
&A_k(\alpha_d, \theta_i + \bar{\vartheta}) \\
&\quad = e^{j\pi\left\{\left[(k-1)d\sin(\theta_i+\bar{\vartheta})/c\right]^2 \sin\alpha_d \cos\alpha_d - 2f_0\cos^2\alpha_d\left[(k-1)d\sin(\theta_i+\bar{\vartheta})/c\right]\right\}} \\
&\quad \cong e^{j\pi\left[((k-1)d\sin(\theta_i)/c)^2 \sin\alpha_d\cos\alpha_d - 2f_0\cos^2\alpha_d((k-1)d\sin(\theta_i)/c)\right]} \\
&\qquad \times e^{j\pi\left[(k-1)^2 d^2\left(2\bar{\vartheta}\sin(\theta_i)\cos(\bar{\vartheta}) + \bar{\vartheta}^2\cos^2(\bar{\vartheta})\right)\sin\alpha_d\cos\alpha_d/c - 2f_0\cos^2\alpha_d\left((k-1)d\bar{\vartheta}\cos(\bar{\vartheta})/c\right)\right]}
\end{aligned} \tag{B4}
$$

Inserting (B4) into (B2), we have

$$b_k = A_k(\alpha_d, \theta_i) G_k(\boldsymbol{\psi}_i), \tag{B5}$$

and

$$\mathbf{b}(\alpha_d, \boldsymbol{\psi}_i) = \mathbf{A}(\alpha_d, \theta_i) \odot \mathbf{G}(\boldsymbol{\psi}_i), \tag{B6}$$

where

$$
\begin{aligned}
&G_k(\boldsymbol{\psi}_i) \\
&\quad = \int_{\bar{\vartheta}\in\bar{\Theta}} e^{j\pi\left[(k-1)^2 d^2\left(2\bar{\vartheta}\sin(\theta_i)\cos(\bar{\vartheta}) + \bar{\vartheta}^2\cos^2(\bar{\vartheta})\right)\sin\alpha_d\cos\alpha_d/c\right]} \\
&\quad \times e^{j\pi\left[-2f_0\cos^2\alpha_d\left((k-1)d\bar{\vartheta}\cos(\bar{\vartheta})/c\right)\right]} \times \ell_i(\theta_i + \bar{\vartheta}, \boldsymbol{\psi}_i) d\bar{\vartheta}
\end{aligned} \tag{B7}
$$

$$\mathbf{G}(\boldsymbol{\psi}_i) = [1, G_2(\boldsymbol{\psi}_i), \cdots, G_r(\boldsymbol{\psi}_i)]^T. \tag{B8}$$

REFERENCES

[1] C. Clemente and J. J. Soraghan, "Range Doppler and chirp scaling processing of synthetic aperture radar data using the fractional Fourier transform," *IET Signal Process.*, vol. 6, no. 5, pp. 503–510, Jul. 2012.

[2] S. A. Elgamel and J. J. Soraghan, "Using EMD-FrFT filtering to mitigate very high power interference in chirp tracking radars," *IEEE Signal Process. Lett.*, vol. 18, no. 4, pp. 263–266, Apr. 2011.

[3] R. Chen and Y. Wang, "Universal FRFT-based algorithm for parameter estimation of chirp signals," *J. Syst. Eng. Electron.*, vol. 18, no. 4, pp. 495–501, Aug. 2012.

[4] K. I. Pedersen, P. E. Mogensen, and B. H. Fleury, "Power azimuth spectrum in outdoor environments," *Electron. Lett.*, vol. 33, no. 18, pp. 1583–1584, Aug.-1997.

[5] P. C. F. Eggers, "Angular propagation descriptions relevant for base station adaptive antenna operations," *Wireless Pers. Commun.*, vol. 11, no. 1, pp. 3–29, Oct. 1999.

[6] S. Valaee, B. Champagne, and P. Kabal, "Parametric localization of distributed sources," *IEEE Trans. Signal Process.*, vol. 43, no. 9, pp. 2144–2153, Sep. 1995.

[7] Y. Meng, P. Stoica, and K. M. Wong, "Estimation of the directions of arrival of spatially dispersed signals in array processing," *IEE Proc.–Radar, Sonar Navigat.*, vol. 143, no. 1, pp. 1–9, Feb. 1996.

[8] B. T. Sieskul, "An asymptotic maximum likelihood for joint estimation of nominal angles and angular spreads of multiple spatially distributed sources," *IEEE Trans. Veh. Technol.*, vol. 59, no. 3, pp. 1534–1538, Mar. 2010.

[9] M. Bengtsson and B. Ottersten, "Low-complexity estimators for distributed sources," *IEEE Trans. Signal Process.*, vol. 48, no. 8, pp. 2185–2194, Aug. 2000.

[10] O. Besson and P. Stoica, "Decoupled estimation of DOA and angular spread for a spatially distributed source," *IEEE Trans. Signal Process.*, vol. 48, no. 7, pp. 1872–1882, Jul. 2000.

[11] E. H. Bae, J. S. Kim, B. W. Choi, and K. K. Lee, "Decoupled parameter estimation of multiple distributed sources for uniform linear array with low complexity," *Electron. Lett.*, vol. 44, no. 10, pp. 649–650, May 2008.

[12] F. Gao and A. B. Gershman, "A generalized esprit approach to direction-of-arrival estimation," *IEEE Signal Process. Lett.*, vol. 12, no. 3, pp. 254–257, Mar. 2005.

[13] J. Yu, L. Zhang, and K. Liu, "Coherently distributed wideband LFM source localization," *IEEE Signal Process. Lett.*, vol. 22, no. 4, pp. 504–508, Apr. 2015.

[14] L. B. Almeida, "The fractional Fourier transform and time-frequency representations," *IEEE Trans. Signal Process.*, vol. 42, no. 11, pp. 3084–3091, Nov. 1994.

[15] H. M. Ozaktas, B. Barshan, D. Mendlovic, L. Onural, "Convolution, filtering, and multiplexing in fractional Fourier domains and their relation to chirp and wavelet transforms," *J. Opt. Soc. Amer. A*, vol. 11, no. 2, pp. 547–559, 1994.

[16] A. W. Lohmann, "Image rotation, Wigner rotation, and the fractional Fourier transform," *J. Opt. Soc. Amer. A*, vol. 10, no. 10, pp. 2181–2186, 1993.

[17] P. Zetterberg, "Mobile cellular communications with base station antenna arrays: Spectrum efficiency, algorithms and propagation models," Ph.D. dissertation, Dept. Signals, Sensors Syst., Royal Inst. Technol., Stockholm, Sweden, 1997.

[18] P. E. Mogensen *et al.*, "Preliminary measurement results from an adaptive antenna array testbed for GSM/UMTS," in *Proc. IEEE 47th Veh. Technol. Conf. Technol. Motion*, May 1997, pp. 1592–1596.

[19] L. Qi, R. Tao, S. Zhou, and Y. Wang, "Detection and parameter estimation of multicomponent LFM signal based on the fractional Fourier transform," *Sci. China Ser. F, Inf. Sci.*, vol. 47, no. 2, pp. 184–198, Mar. 2004.

[20] P. Stoica and A. Nehorai, "MUSIC, maximum likelihood, and Cramer–Rao bound," *IEEE Trans. Acoust., Speech, Signal Process.*, vol. 37, no. 5, pp. 720–741, May 1989.

[21] P. Stoica and A. Nehorai, "Performance study of conditional and unconditional direction-of-arrival estimation," *IEEE Trans. Acoust., Speech, Signal Process.*, vol. 38, no. 10, pp. 1783–1795, Oct. 1990.

[22] P. Stoica, E. G. Larsson, and A. B. Gershman, "The stochastic CRB for array processing: A textbook derivation," *IEEE Signal Process. Lett.*, vol. 8, no. 5, pp. 148–150, May 2001.

[23] H. M. Ozaktas, O. Arikan, M. A. Kutay, and G. Bozdagt, "Digital computation of the fractional Fourier transform," *IEEE Trans. Signal Process.*, vol. 44, no. 9, pp. 2141–2150, Sep. 1996.

[24] F. Liu, H. Xu, R. Tao, and Y. Wang, "Research on resolution between multi-component LFM signals in the fractional Fourier domain," *Sci. China Inf. Sci.*, vol. 55, no. 6, pp. 1301–1312, Jun. 2012.

[25] P. Luo, K.-H. Liu, W.-G. Shi, and G. Yan, "2-D DOA estimation of wideband LFM signals for arbitrary planar array," in *Proc. IEEE 10th Int. Conf. Signal Process.*, Dec. 2010, pp. 307–310.

[26] Z. Zhao and C. Liu, "Joint estimation of time-frequency signature and DOA based on STFD for multicomponent Chirp signals," *Int. Scholarly Res. Notices*, vol. 2014, Nov. 2014. [Online]. Available: https://www.hindawi.com/journals/isrn/2014/937139/

LIANG ZHANG was born in Tianjin, China. He received the M.S. degree in information and communication engineering and the Ph.D. degree in circuits and systems from Tianjin University, Tianjin, China. He is currently a Lecturer with the Civil Aviation University of China, Tianjin. His research areas include array signal processing, localization, and deep learning and its applications.

YANBEI LIU received the B.E. degree from the Zhengzhou University of Light Industry, Zhengzhou, China, in 2009, the M.E. degree from Tianjin Polytechnic University, Tianjin, China, in 2012, and the Ph.D. degree from Tianjin University, Tianjin, in 2017. He is currently a Lecturer with Tianjin Polytechnic University. His current research interests include machine learning, data mining, and computer vision.

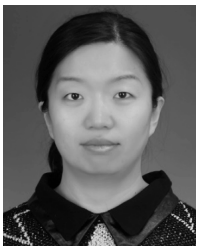

JIEXIAO YU (M'15) was born in Tianjin, China. She received the B.S. degree in electronic information engineering from Nankai University in 2002 and the M.S. degree in theory and new technology of electrical engineering and the Ph.D. degree in circuits and systems from Tianjin University, Tianjin, China, in 2005 and 2009, respectively. She is currently an Associate Professor with the School of Electrical and Information Engineering (previously known as the School of Electronic Information Engineering), Tianjin University. Her current research interests include wireless localization, RFID, WSN, and array signal processing.

KAIHUA LIU was born in Tianjin, China. He received the B.S. degree in semiconductor physics and devices, the M.S. degree in circuits and systems, and the Ph.D. degree in signal processing from Tianjin University, Tianjin, China, in 1981, 1991, and 1999, respectively. He is currently a Professor with the School of Electronic Information Engineering, Tianjin University. His current research interests include wireless localization and communication.